Commun. Comput. Phys.
doi: 10.4208/cicp.OA-2017-0114

Vol. **24**, No. 5, pp. 1279-1299
November 2018

An Improved Formulation for Hybridizable Discontinuous Galerkin Fluid-Structure Interaction Modeling with Reduced Computational Expense

Jason P. Sheldon[1], Scott T. Miller[2] and Jonathan S. Pitt[1,*]

[1] *Applied Research Laboratory, The Pennsylvania State University, University Park, PA 16802, USA.*
[2] *Sandia National Laboratories, Albuquerque, NM 87185, USA.*

Received 17 May 2017; Accepted (in revised version) 3 November 2017

Abstract. This work presents two computational efficiency improvements for the hybridizable discontinuous Galerkin (HDG) fluid-structure interaction (FSI) model presented by Sheldon et al. A new formulation for the solid is presented that eliminates the global displacement, resulting in the velocity being the only global solid variable. This necessitates a change to the solid-mesh displacement coupling, which is accounted for by coupling the local solid displacement to the global mesh displacement. Additionally, the mesh basis and test functions are restricted to linear polynomials, rather than being equal-order with the fluid and solid. This change increases the computational efficiency dynamically, with greater benefit the higher order the computation, when compared to an equal-order formulation. These two improvements result in a 50% reduction in the number of global degrees of freedom for high-order simulations for both the fluid and solid domains, as well as an approximately 50% reduction in the number of local fluid domain degrees of freedom for high-order simulations. The new, more efficient formulation is compared against that from Sheldon et al. and negligible change of accuracy is found.

AMS subject classifications: 65M60, 74F10

Key words: Hybridizable discontinuous Galerkin, fluid-structure interaction, HDG FSI, monolithic coupling, arbitrary Lagrangian-Eulerian Navier-Stokes, elastodynamics.

1 Introduction

Many natural phenomena, such as blood transport or aeroelastic flutter [1], require tightly coupled fluid-structure interaction (FSI) simulations to accurately represent the complex multi-physics. FSI simulations, particularly those involving large amplitude, low

*Corresponding author. *Email addresses:* jsp203@psu.edu (J. S. Pitt), jasonpsheldon@gmail.com (J. P. Sheldon), stmille@sandia.gov (S. T. Miller)

frequency, solid deformation, are substantially more computationally expensive and difficult to model than traditional fluid-only or solid-only simulations due to the tight coupling on fluid-solid interface and the disparate mathematics used to describe the fluid and solid regions in the models [2]. With the goal of reducing the computational expense associated with FSI simulations, the hybridizable discontinuous Galerkin (HDG) method was first utilized for FSI simulation by Sheldon et al. [3, 4]. The HDG method is a recently developed finite element method that has the benefits of discontinuous Galerkin (DG) methods, such as scalability in parallel, local conservation of variables, stability with complicated geometries, and high-order accuracy based on the degree of the approximating polynomial [5], while reducing the high computational cost associated with DG methods [6]. This reduction is achieved by separation (hybridization) of the solution into local element solutions and global trace solutions on the element interfaces. This minimizes the number of globally coupled degrees of freedom (DOFs), along with the computational cost of solving the global system, while preserving the benefits of DG methods. Only the primary variable of interest, referred to as the hybrid unknown, exists in both the local and global solution spaces, and it is the only unknown solved for globally, i.e., across the entire mesh, in this formulation. The individual local variables can be solved in an inherently parallel fashion, being completely decoupled from one another.

This work does not focus on deriving formulations with the HDG method or on FSI in general. For more on these topics, please see Sheldon et al. [3,4,7]. Additionally, Nguyen et al. present an excellent introduction to the HDG method in [8] for Stokes flow and in [9] for an overview to a wide variety of physics. Extensive literature exists on a multitude of other computational methods for FSI, e.g. [10–12], and the interested reader is referred to the references therein for further information. This work also does not tackle many of the items identified as future work for HDG FSI in [3,4,7], including: higher order post-processing, the non-linear solid strain's suboptimal convergence rate, parallel processing scaling and efficiency studies, investigation of optimal stabilization parameters for HDG multiphysics, and a full three-dimensional HDG FSI study. These remain interesting and important areas of future work, each worthy of their own investigation.

Instead, the focus of this work is a reduction in the number of DOFs for the HDG FSI system and the resultant increase in computational efficiency over the formulations presented in [3, 4]. Two factors contribute to this DOF reduction. First, the global solid displacement is eliminating from the solid formulation. This has repercussions on the solid-mesh FSI coupling that are discussed later. Second, the function spaces for the mesh test and basis functions are restricted to linear polynomials, regardless of the order of the rest of the simulation. The computational effects of these two changes is a 50% reduction in the number of global DOFs for high-order simulations across both the fluid and solid domains, as well as an approximately 50% reduction in the number of local fluid domain DOFs for high-order simulations. The specific DOF reductions versus simulation order are detailed in Appendix A and Table 4.

In the following section a brief background of the mathematics necessary for HDG FSI modeling is presented. Next, the fluid, solid, and mesh formulations from [3, 4] are

reproduced, but not derived (see [3, 4] for full derivation), and then the modifications to these formulations discussed above are presented. With the new formulations, the same code-to-code comparisons performed in [3, 4] are repeated and the results are shown to be indistinguishable, except for a substantial DOF reduction. Finally, a brief discussion of stability is presented along with some concluding remarks.

2 Background mathematics

A mathematical model of FSI requires governing equations for both fluid systems and solid systems, along with the coupling that combines them. The fluid formulation presented herein is the unsteady incompressible Navier-Stokes equations, cast into the Arbitrary Lagrangian Eulerian (ALE) framework. For the solid equations, a Saint Venant-Kirchhoff non-linear elastodynamics formulation is presented, while a linear elastostatics formulation is used for mesh motion. This last formulation, with arbitrary (user chosen) material properties, is used to update the computational domain on which the fluid is solved (necessary for the ALE Navier-Stokes formulation). Before these formulations themselves can be presented, a certain level of background information is necessary.

2.1 Kinematics

The modeling process for fluids and solids is very similar; however, there are some differences that need to be addressed. Fluid equations are typically written in the Eulerian (deformed) reference frame, while solid equations are generally written in the Lagrangian (referential) reference frame. There is a disconnect between these frames on the fluid-solid interface that can be accounted for in various ways, such as the immersed boundary method [13, 14] or the ALE method [15, 16]. In this work, the ALE formulation is used for the fluid, which accounts for the change in frame by transforming the standard Eulerian governing differential equations into a form defined on the reference configuration $\Omega_F(0)$. There are many references that provide more details on kinematics and reference frames, such as Gurtin [17] or Spencer [18]; however, for this work it is worth specifically noting the following.

The position of a material point in some reference body β_κ (before deformation) is $\mathbf{X}$, while the position of a material point in a deformed configuration β, known as the spatial point, is $\mathbf{x}$. The deformation function $\chi(\mathbf{X},t)$ maps a material point $\mathbf{X}$ to the spatial point $\mathbf{x}$ at the instant of time t. Considering a smooth sequence of configurations ordered in time, a motion is defined as

$$\chi(\mathbf{X},t)=\mathbf{x}(\mathbf{X},t)=\mathbf{X}+\mathbf{u}, \tag{2.1}$$

where $\mathbf{u}$ is the displacement vector, given by

$$\mathbf{u}=\mathbf{x}(\mathbf{X},t)-\mathbf{X}. \tag{2.2}$$

Operators with capitalized first letters (e.g. Grad) denote differential operators with respect to the referential/material coordinate $\mathbf{X}$, while those with lower-case first letters (e.g. grad) denote differential operators with respect to the spatial/deformed coordinate $\mathbf{x}$. The deformation-gradient can be expressed as

$$\mathbf{F}(\mathbf{X},t) = \mathrm{Grad}\,\chi = \mathbf{I} + \mathrm{Grad}\,\mathbf{u}, \tag{2.3}$$

and the determinant of $\mathbf{F}$ is

$$J = \det(\mathbf{F}). \tag{2.4}$$

In Section 3.1, $\mathbf{F}$ and J are used for push-forward and pull-back operations in the ALE description of the fluid region.

2.2 FSI

For FSI, the displacement vector is piecewise defined over the solid and fluid subregions as

$$\mathbf{u} = \begin{cases} \mathbf{u}_\mathrm{s}, & \forall \mathbf{X} \in \Omega_\mathrm{S}, \\ \mathbf{u}_\mathrm{m}, & \forall \mathbf{X} \in \Omega_\mathrm{F}, \end{cases} \tag{2.5}$$

where Ω_S is the solid subdomain, Ω_F is the fluid subdomain, $\mathbf{u}_\mathrm{s}$ is the solid displacement and $\mathbf{u}_\mathrm{m}$ is the (arbitrary) displacement of the (mesh) fluid subdomain. The displacement of the fluid subdomain is governed by the mesh motion, hence the subscript "m" and not "f", where the subscripts "m", "s", and "f" refer to "mesh", "solid", and "fluid" respectively. Continuity of displacement on the fluid-solid interface requires

$$\mathbf{u}_\mathrm{s} - \mathbf{u}_\mathrm{m} = \mathbf{0}, \quad \forall \mathbf{X} \in \Gamma_\mathrm{FS}, \tag{2.6}$$

where $\Gamma_\mathrm{FS} = \Omega_\mathrm{S} \cap \Omega_\mathrm{F}$ is the interface between the solid and fluid subdomains.

2.3 Spatial discretization

Regardless of the differential equations being solved, the process of spatial discretization is always roughly the same. Given an arbitrary spatial domain Ω over which some governing equation should be solved, break that domain into a sufficiently regular collection $\mathcal{T}^\mathrm{h}$ of disjoint elements K, with faces F. This collection defines the mesh, or triangulation, which serves as a model for the original domain. The governing equations, written in their strong form, have their primary variables approximated by discretized counterparts, are weighted with some arbitrary function, and are integrated over their respective domains, resulting in the weak form of the governing equations. Typically, the test functions (indicated with a tilde) and basis functions for the approximated primary variables (indicated with a superscript $^\mathrm{h}$) are chosen from the same finite dimensional solution spaces. An example space for some discretized variable $\mathbf{a}^\mathrm{h}$ is

$$A^\mathrm{h} := \left\{ \mathbf{a}^\mathrm{h} \in \left[L^2\left(\mathcal{T}^\mathrm{h}\right) \right]^d : \left. \mathbf{a}^\mathrm{h} \right|_K \in [P_k(K)]^d, \quad \forall K \in \mathcal{T}^\mathrm{h} \right\}, \tag{2.7}$$

where d is the dimension of a given space, $P_k(K)$ denotes the space of polynomials of at most degree k on element K, and $L^2(K)$ denotes the space of square integrable functions on K.

2.4 Temporal discretization

Temporal discretization is not the focus of this work. See [19] (or many other sources) for derivation, discussion, and presentation of a variety of temporal discretization methods. All results presented in this work use the second-order backwards difference formula (BFD2), which approximates the solution to

$$\frac{\mathrm{d}\mathbf{y}(t)}{\mathrm{d}t} = \mathbf{f}(\mathbf{y}(t), t), \tag{2.8}$$

as

$$3\mathbf{y}_{n+2} - 4\mathbf{y}_{n+1} + \mathbf{y}_n = 2\Delta t \mathbf{f}(t_{n+2}), \tag{2.9}$$

where the subscripts indicate information from various timestep levels.

3 Fluid-structure interaction model

In this section the model for HDG FSI is presented. First, the fluid governing equations are presented in their ALE form, while the mesh and solid governing equation are presented in their Lagrangian forms. Second, the constraints necessary for FSI coupling are discussed and the function spaces for the discretized variables are presented. Finally, the HDG formulations from [3,4] are reproduced along with their DOF reduced counterparts. The derivations for the following formulations are only presented when derivations differ from those presented in [3, 4]. Commentary is made throughout the entire section on the changes necessary for the DOF reduction. The formulations in this section loosely follow the work of Nguyen et al. [9, 20], Soon et al. [21], and Kronbichler et al. [22], with specific attributions given in the full derivations found in [3, 4].

3.1 Governing equations

3.1.1 ALE formulation of Navier-Stokes equations

Presented below are the strong forms of the ALE incompressible Navier-Stokes equations, including the conservation of linear momentum, a kinematic compatibility equation for the velocity-gradient, the continuity equation, and appropriate boundary conditions. The primary fluid variables being solved for are the velocity $\mathbf{v}$ (hybrid), the

pressure p, and the velocity gradient $\mathbf{L}$.

$$\rho_{\mathrm{f}}\frac{\partial \mathbf{v}_{\mathrm{f}}}{\partial t}+\rho_{\mathrm{f}}\mathbf{L}_{\mathrm{f}}[\mathbf{v}_{\mathrm{f}}-\mathbf{v}_{\mathrm{m}}]+\mathrm{Grad}\,(p_{\mathrm{f}}\mathbf{I}-\mu_{\mathrm{f}}\mathbf{L}_{\mathrm{f}}):\mathbf{F}_{\mathrm{m}}^{-\mathsf{T}}=\mathbf{f}_{\mathrm{f}} \qquad \forall \mathbf{X}\in\Omega_{\mathrm{F}}(0), \tag{3.1}$$

$$\mathbf{L}_{\mathrm{f}}-\mathrm{Grad}\,\mathbf{v}_{\mathrm{f}}\mathbf{F}_{\mathrm{m}}^{-1}=\mathbf{0} \qquad \forall \mathbf{X}\in\Omega_{\mathrm{F}}(0), \tag{3.2}$$

$$\mathbf{F}_{\mathrm{m}}^{-\mathsf{T}}\colon \mathrm{Grad}\,\mathbf{v}_{\mathrm{f}}=0 \qquad \forall \mathbf{X}\in\Omega_{\mathrm{F}}(0), \tag{3.3}$$

$$\mathbf{v}_{\mathrm{f}}=\mathbf{g}_{\mathrm{D_f}} \qquad \forall \mathbf{X}\in\Gamma_{\mathrm{D_F}}(0), \tag{3.4}$$

$$(p_{\mathrm{f}}\mathbf{I}-\mu_{\mathrm{f}}\mathbf{L}_{\mathrm{f}})\mathbf{F}_{\mathrm{m}}^{-\mathsf{T}}[\mathbf{n}_{\mathrm{f}}]=\mathbf{g}_{\mathrm{N_f}} \qquad \forall \mathbf{X}\in\Gamma_{\mathrm{N_F}}(0). \tag{3.5}$$

3.1.2 Linear elastostatics formulation (mesh motion)

For mesh motion, a linear elastostatics formulation is used, with arbitrary (user defined) material properties. The primary variables of displacement $\mathbf{u}$ (hybrid) and deformation gradient $\mathbf{F}$ are chosen for their convenience in the ALE fluid formulation in FSI. With these primary variables, linear elastostatics is governed by the steady form of the conservation of linear momentum, written in the Lagrangian reference frame, along with a constitutive relation for deformation-gradient and appropriate boundary conditions:

$$-\mathrm{Div}\,\mathbb{C}_{\mathrm{m}}[\mathbf{F}_{\mathrm{m}}-\mathbf{I}]=\mathbf{f}_{\mathrm{m}} \qquad \forall \mathbf{X}\in\Omega_{\mathrm{F}}(0), \tag{3.6}$$

$$\mathbf{F}_{\mathrm{m}}-\mathbf{I}-\mathrm{Grad}\,\mathbf{u}_{\mathrm{m}}=\mathbf{0} \qquad \forall \mathbf{X}\in\Omega_{\mathrm{F}}(0), \tag{3.7}$$

$$\mathbf{u}_{\mathrm{m}}=\mathbf{g}_{\mathrm{D_m}} \qquad \forall \mathbf{X}\in\Gamma_{\mathrm{D_F}}(0), \tag{3.8}$$

$$(\mathbb{C}_{\mathrm{m}}[\mathbf{F}_{\mathrm{m}}-\mathbf{I}])[\mathbf{n}_{\mathrm{m}}]=\mathbf{g}_{\mathrm{N_m}} \qquad \forall \mathbf{X}\in\Gamma_{\mathrm{N_F}}(0), \tag{3.9}$$

where $\mathbb{C}_{\mathrm{m}}$ is the elasticity tensor with arbitrary mesh material properties.

3.1.3 Nonlinear elastodynamics formulation

The (geometrically) nonlinear Saint Venant-Kirchhoff model was used in [3, 4] because it was the model Turek and Hron used for their FSI benchmark [23], with which these formulations are compared in Section 4. In [3,4] the primary variables were the displacement $\mathbf{u}$ (hybrid), the velocity $\mathbf{v}$ (hybrid) and the Green-St. Venant strain $\mathbf{E}$; however, in this work, only the velocity is a hybrid variable, which requires changes to the governing equations. First, the strong form from [3,4] is presented, which is analogous to the system for linear elastostatics, but with an additional kinematic compatibility condition:

$$\rho\frac{\partial \mathbf{v}_{\mathrm{s}}}{\partial t}-\mathrm{Div}\,[\mathbf{F}_{\mathrm{s}}\mathbb{C}_{\mathrm{s}}(\mathbf{E}_{\mathrm{s}})]=\mathbf{f}_{\mathrm{s}} \qquad \forall \mathbf{X}\in\Omega_{\mathrm{S}}, \tag{3.10}$$

$$\mathbf{E}_{\mathrm{s}}-\tfrac{1}{2}\left(\mathrm{Grad}\,\mathbf{u}_{\mathrm{s}}+(\mathrm{Grad}\,\mathbf{u}_{\mathrm{s}})^{\mathsf{T}}+(\mathrm{Grad}\,\mathbf{u}_{\mathrm{s}})^{\mathsf{T}}\mathrm{Grad}\,\mathbf{u}_{\mathrm{s}}\right)=0 \qquad \forall \mathbf{X}\in\Omega_{\mathrm{S}}, \tag{3.11}$$

$$\frac{\partial \mathbf{u}_{\mathrm{s}}}{\partial t}=\mathbf{v}_{\mathrm{s}} \qquad \forall \mathbf{X}\in\Omega_{\mathrm{S}}, \tag{3.12}$$

$$\mathbf{u}=\mathbf{g}_{\mathrm{D_s}} \qquad \forall \mathbf{X}\in\Gamma_{\mathrm{D_S}}, \tag{3.13}$$

$$[\mathbf{F}_{\mathrm{s}}\mathbb{C}_{\mathrm{s}}(\mathbf{E}_{\mathrm{s}})][\mathbf{n}]=\mathbf{g}_{\mathrm{N_s}} \qquad \forall \mathbf{X}\in\Gamma_{\mathrm{N_S}}, \tag{3.14}$$

where $\mathbb{C}_s$ is the elasticity tensor for the solid's material properties. The solid deformation tensor $\mathbf{F}_s = \mathbf{I} + \text{Grad}\,\mathbf{u}_s$ is not a primary variable, but it is shown in the formulation for brevity.

Having a two-hybrid-field formulation is not desirable for several reasons, with the most important reason being that it increases the number of global DOFs, which is contrary to the entire point of the HDG method. At the time [3, 4] were written, no alternative to a two-hybrid-field solid formulation was thought possible; however that has since changed. In order to write a one-hybrid-field solid formulation, Eq. (3.11) must be differentiated with respect to time and Eq. (3.13) must be written in terms of velocity, resulting in

$$\frac{\partial \mathbf{E}_s}{\partial t} - \text{Sym}(\text{Grad}\,\mathbf{v}_s) + \tfrac{1}{2}\left[(\text{Grad}\,\mathbf{v}_s)^{\mathsf{T}}\text{Grad}\,\mathbf{u}_s + (\text{Grad}\,\mathbf{u}_s)^{\mathsf{T}}\text{Grad}\,\mathbf{v}_s\right] = 0 \qquad \forall \mathbf{X} \in \Omega_S, \quad (3.15)$$

$$\mathbf{v} = \mathbf{g}_{D_s} \qquad \forall \mathbf{X} \in \Gamma_{D_S}. \quad (3.16)$$

No other changes to the strong form of the equations are necessary, but more changes will be presented for both the FSI coupling and the weak forms of the solid and mesh governing equations in the following sections.

3.2 FSI Coupling

To couple these three formulations together for monolithic FSI, the system requires three conditions on the fluid-solid interface: the solid displacement governs the mesh displacement, the solid and fluid velocity fields are continuous, and finally, the solid and fluid tractions are continuous. For the HDG method, boundary (or interface) conditions need to be applied to the solution trace (the global variables). This was the reason for the two-hybrid-field solid formulation presented in [3, 4]. Those boundary conditions are reproduced below, and then the modification for a one-hybrid-field solid formulation is discussed:

$$(\boldsymbol{\mu}_m - \boldsymbol{\mu}_s)\Big|_{\Gamma_{FS}} = \mathbf{0}, \quad (3.17)$$

$$(\boldsymbol{v}_s - \boldsymbol{v}_f)\Big|_{\Gamma_{FS}} = \mathbf{0}, \quad (3.18)$$

$$\left(\widehat{\mathbf{T}}_s[\mathbf{n}_s] + \widehat{\mathbf{T}}_f[\mathbf{n}_f]\right)\Big|_{\Gamma_{FS}} = \mathbf{0}, \quad (3.19)$$

where $\boldsymbol{\mu}$, $\boldsymbol{v}$, and $\widehat{\mathbf{T}}$ are the global components of the displacement, velocity and traction respectively. The orientation of the fluid-solid interface Γ_{FS} requires $\mathbf{n}_s = -\mathbf{n}_f$. Section 3.4 discusses how the global traction is approximated in terms of the other variables to reduce the number of global unknowns.

Unlike the velocity and traction conditions, which are two-way coupled, the solid-mesh displacement condition (3.17) must be one-way coupled. The mesh should not directly influence the solid because the mesh is non-physical and its properties are arbitrary,

otherwise the artificial mesh 'stiffness' would limit the motion of the solid. Therefore, the solid-mesh displacement condition (3.17) must be added to the mesh governing equations on the interface, but not to the solid governing equations. Due to this restriction, it is possible to rewrite Eq. (3.17) in terms of the global mesh displacement, but only the *local* solid displacement:

$$(\boldsymbol{\mu}_{\mathrm{m}}-\mathbf{u}_{\mathrm{s}})\Big|_{\Gamma_{\mathrm{FS}}}=\mathbf{0}, \tag{3.20}$$

which is the entire reason a one-hybrid-field solid formulation is possible.

3.3 Function spaces

The discontinuous finite element approximation spaces for the discrete fluid, solid, and mesh subproblems presented in [3, 4] were chosen from the spaces reproduced below. The test functions are chosen from the same respective spaces as the discretized primary variables, except for those with Dirichlet boundary conditions. These spaces, as with all the basis functions in this document, are indicated with a tilde.

$$\begin{aligned}
\boldsymbol{U}_{\mathrm{m,s}}^{\mathrm{h}} &:= \left\{ \mathbf{u}_{\mathrm{m,s}}^{\mathrm{h}} \in \left[L^2\left(\mathcal{T}_{\mathrm{f,s}}^{\mathrm{h}}\right)\right]^d : \ \mathbf{u}_{\mathrm{m,s}}^{\mathrm{h}}\Big|_K \in [P_k(K)]^d, \quad \forall K \in \mathcal{T}_{\mathrm{f,s}}^{\mathrm{h}} \right\}, \\
\boldsymbol{V}_{\mathrm{f,s}}^{\mathrm{h}} &:= \left\{ \mathbf{v}_{\mathrm{f,s}}^{\mathrm{h}} \in \left[L^2\left(\mathcal{T}_{\mathrm{f,s}}^{\mathrm{h}}\right)\right]^d : \ \mathbf{v}_{\mathrm{f,s}}^{\mathrm{h}}\Big|_K \in [P_k(K)]^d, \quad \forall K \in \mathcal{T}_{\mathrm{f,s}}^{\mathrm{h}} \right\}, \\
\boldsymbol{\mathcal{E}}_{\mathrm{s}}^{\mathrm{h}} &:= \left\{ \mathbf{E}_{\mathrm{s}}^{\mathrm{h}} \in \left[L^2\left(\mathcal{T}_{\mathrm{s}}^{\mathrm{h}}\right)\right]^{d\times d} : \ \mathbf{E}_{\mathrm{s}}^{\mathrm{h}}\Big|_K \in [P_k(K)]^{d\times d}, \quad \forall K \in \mathcal{T}_{\mathrm{s}}^{\mathrm{h}} \right\}, \\
\boldsymbol{\mathcal{F}}_{\mathrm{m}}^{\mathrm{h}} &:= \left\{ \mathbf{F}_{\mathrm{m}}^{\mathrm{h}} \in \left[L^2\left(\mathcal{T}_{\mathrm{f}}^{\mathrm{h}}\right)\right]^{d\times d} : \ \mathbf{F}_{\mathrm{m}}^{\mathrm{h}}\Big|_K \in [P_k(K)]^{d\times d}, \quad \forall K \in \mathcal{T}_{\mathrm{f}}^{\mathrm{h}} \right\}, \\
\boldsymbol{\mathcal{L}}_{\mathrm{f}}^{\mathrm{h}} &:= \left\{ \mathbf{L}_{\mathrm{f}}^{\mathrm{h}} \in \left[L^2\left(\mathcal{T}_{\mathrm{f}}^{\mathrm{h}}\right)\right]^{d\times d} : \ \mathbf{L}_{\mathrm{f}}^{\mathrm{h}}\Big|_K \in [P_k(K)]^{d\times d}, \quad \forall K \in \mathcal{T}_{\mathrm{f}}^{\mathrm{h}} \right\}, \\
\mathcal{P}_{\mathrm{f}}^{\mathrm{h}} &:= \left\{ p_{\mathrm{f}}^{\mathrm{h}} \in L^2\left(\mathcal{T}_{\mathrm{f}}^{\mathrm{h}}\right) : \ p_{\mathrm{f}}^{\mathrm{h}}\Big|_K \in P_k(K), \quad \forall K \in \mathcal{T}_{\mathrm{f}}^{\mathrm{h}} \right\}, \\
\boldsymbol{M}_{\mathrm{m,s}}^{\mathrm{h}} &:= \left\{ \boldsymbol{\mu}_{\mathrm{m,s}}^{\mathrm{h}} \in \left[L^2\left(\mathcal{F}_{\mathrm{f,s}}^{\mathrm{h}}\right)\right]^d : \ \boldsymbol{\mu}_{\mathrm{m,s}}^{\mathrm{h}}\Big|_F \in [P_k(F)]^d, \quad \forall F \in \mathcal{F}_{\mathrm{f,s}}^{\mathrm{h}}, \boldsymbol{\mu}_{\mathrm{m,s}}^{\mathrm{h}}\big|_{\partial\Omega_{\mathrm{D_{f,s}}}} = \mathbf{g}_{\mathrm{D_{m,s}}} \right\}, \\
\widetilde{\boldsymbol{M}}_{\mathrm{m,s}} &:= \left\{ \widetilde{\boldsymbol{\mu}}_{\mathrm{m,s}} \in \left[L^2\left(\mathcal{F}_{\mathrm{f,s}}^{\mathrm{h}}\right)\right]^d : \ \widetilde{\boldsymbol{\mu}}_{\mathrm{m,s}}|_F \in [P_k(F)]^d, \quad \forall F \in \mathcal{F}_{\mathrm{f,s}}^{\mathrm{h}}, \widetilde{\boldsymbol{\mu}}_{\mathrm{m,s}}\big|_{\partial\Omega_{\mathrm{D_{f,s}}}} = 0 \right\}, \\
\boldsymbol{\mathcal{V}}_{\mathrm{f,s}}^{\mathrm{h}} &:= \left\{ \boldsymbol{v}_{\mathrm{f,s}}^{\mathrm{h}} \in \left[L^2\left(\mathcal{F}_{\mathrm{f,s}}^{\mathrm{h}}\right)\right]^d : \ \boldsymbol{v}_{\mathrm{f,s}}^{\mathrm{h}}\Big|_F \in [P_k(F)]^d, \quad \forall F \in \mathcal{F}_{\mathrm{f,s}}^{\mathrm{h}}, \boldsymbol{v}_{\mathrm{f}}^{\mathrm{h}}\big|_{\partial\Omega_{\mathrm{D_f}}} = \mathbf{g}_{\mathrm{D_f}} \right\}, \\
\widetilde{\boldsymbol{\mathcal{V}}}_{\mathrm{f,s}} &:= \left\{ \widetilde{\boldsymbol{v}}_{\mathrm{f,s}} \in \left[L^2\left(\mathcal{F}_{\mathrm{f,s}}^{\mathrm{h}}\right)\right]^d : \ \widetilde{\boldsymbol{v}}_{\mathrm{f,s}}|_F \in [P_k(F)]^d, \quad \forall F \in \mathcal{F}_{\mathrm{f,s}}^{\mathrm{h}}, \widetilde{\boldsymbol{v}}_{\mathrm{f,s}}\big|_{\partial\Omega_{\mathrm{D_{f,s}}}} = 0 \right\}, \\
\Psi_{\mathrm{f}}^{\mathrm{h}} &:= \left\{ \psi_{\mathrm{f}}^{\mathrm{h}} \in L^2\left(\mathcal{T}_{\mathrm{f}}^{\mathrm{h}}\right) : \ \psi_{\mathrm{f}}^{\mathrm{h}}\Big|_K \in P_0(K), \quad \forall K \in \mathcal{T}_{\mathrm{f}}^{\mathrm{h}} \right\},
\end{aligned} \tag{3.21}$$

where $\mathcal{F}^h$ is the set of all faces, for all elements in $\mathcal{T}^{\mathrm{h}}$. In order to reduce the number of total DOFs (both local and global), the basis and test functions for the mesh variables

are restricted to only linear polynomials. Additionally, because of the changes made in Eq. (3.16), the space for the global velocity must now include a Dirichlet condition for the solid. These new spaces are presented below, and they replace the respective spaces from Eq. (3.21) for the new reduced DOF formulation.

$$
\begin{aligned}
\boldsymbol{U}_{\mathrm{m}}^{1} &:= \left\{ \mathbf{u}_{\mathrm{m}}^{\mathrm{h}} \in \left[L^2\left(\mathcal{T}_{\mathrm{f}}^{\mathrm{h}}\right) \right]^d : \ \mathbf{u}_{\mathrm{m}}^{\mathrm{h}}\Big|_K \in [P_1(K)]^d, \quad \forall K \in \mathcal{T}_{\mathrm{f}}^{\mathrm{h}} \right\}, \\
\boldsymbol{\mathcal{F}}_{\mathrm{m}}^{1} &:= \left\{ \mathbf{F}_{\mathrm{m}}^{\mathrm{h}} \in \left[L^2\left(\mathcal{T}_{\mathrm{f}}^{\mathrm{h}}\right) \right]^{d\times d} : \ \mathbf{F}_{\mathrm{m}}^{\mathrm{h}}\Big|_K \in [P_1(K)]^{d\times d}, \quad \forall K \in \mathcal{T}_{\mathrm{f}}^{\mathrm{h}} \right\}, \\
\boldsymbol{M}_{\mathrm{m}}^{1} &:= \left\{ \boldsymbol{\mu}_{\mathrm{m}}^{\mathrm{h}} \in \left[L^2\left(\mathcal{F}_{\mathrm{f}}^{\mathrm{h}}\right) \right]^d : \ \boldsymbol{\mu}_{\mathrm{m}}^{\mathrm{h}}\Big|_F \in [P_1(F)]^d, \quad \forall F \in \mathcal{F}_{\mathrm{f}}^{\mathrm{h}}, \boldsymbol{\mu}_{\mathrm{m}}^{\mathrm{h}}\big|_{\partial\Omega_{\mathrm{D_f}}} = \mathbf{g}_{\mathrm{D_m}} \right\}, \\
\widetilde{\boldsymbol{M}}_{\mathrm{m}}^{1} &:= \left\{ \widetilde{\boldsymbol{\mu}}_{\mathrm{m}} \in \left[L^2\left(\mathcal{F}_{\mathrm{f}}^{\mathrm{h}}\right) \right]^d : \ \widetilde{\boldsymbol{\mu}}_{\mathrm{m}}|_F \in [P_1(F)]^d, \quad \forall F \in \mathcal{F}_{\mathrm{f}}^{\mathrm{h}}, \widetilde{\boldsymbol{\mu}}_{\mathrm{m}}\big|_{\partial\Omega_{\mathrm{D_f}}} = 0 \right\}, \\
\boldsymbol{\mathcal{V}}_{\mathrm{f,s}}^{\mathrm{h}} &:= \left\{ \boldsymbol{v}_{\mathrm{f,s}}^{\mathrm{h}} \in \left[L^2\left(\mathcal{F}_{\mathrm{f,s}}^{\mathrm{h}}\right) \right]^d : \ \boldsymbol{v}_{\mathrm{f,s}}^{\mathrm{h}}\Big|_F \in [P_k(F)]^d, \quad \forall F \in \mathcal{F}_{\mathrm{f,s}}^{\mathrm{h}}, \boldsymbol{v}_{\mathrm{f,s}}^{\mathrm{h}}\big|_{\partial\Omega_{\mathrm{D_{f,s}}}} = \mathbf{g}_{\mathrm{D_{f,s}}} \right\}.
\end{aligned}
\tag{3.22}
$$

The restrictions from the mesh function space result in a variable local and global fluid domain DOF reduction up to approximately 50% for high-order problems. This is demonstrated in Appendix A. The accuracy of the solution is not affected by restricting the mesh function spaces to linear polynomials because the mesh is a non-physical construct used solely for the ALE transformation. The mesh only has two requirements: that it satisfies all the boundary conditions[†] and that is sufficiently smooth. Linear polynomials meet both of these requirements, and so using higher-order polynomials is wasteful in terms of computational resources. In fact, as is discussed later, the only other side effect of the restricted mesh function spaces appears to be increased stability. The numerical studies for this work using linear function spaces for the mesh variables had a more stable solution than those with equal-order mesh function spaces.

3.4 HDG discretization for FSI sub-problems

The HDG discretization procedure for the three sets of governing equations from Section 3.1 is presented in full in [3, 4]. In this section, the final HDG formulations are reproduced along with a discussion of the differences pertaining to the one-hybrid-field solid formulation.

3.4.1 Fluid

The fluid governing equations are entirely unchanged from [3, 4]. The discretized primary variables for the ALE Navier-Stokes formulation are the velocity-gradient $\mathbf{L}_{\mathrm{f}}^{\mathrm{h}}$, the velocity $\mathbf{v}_{\mathrm{f}}^{\mathrm{h}}$, the pressure $p_{\mathrm{f}}^{\mathrm{h}}$, the trace of the velocity over the element faces $\boldsymbol{v}_{\mathrm{f}}^{\mathrm{h}}$, and the

[†]For a complex fluid-solid interface, it may be desirable to use equal-order mesh function spaces specifically on the interface to preserve displacement continuity between the solid and mesh. This should not substantially increase the number overall DOFs, but is worth noting.

mean pressure over each element $\psi_{\mathrm{f}}^{\mathrm{h}}$. Each has an associated test function: $\widetilde{\mathbf{L}}_{\mathrm{f}}$, $\widetilde{\mathbf{v}}_{\mathrm{f}}$, $\widetilde{p}_{\mathrm{f}}$, $\widetilde{\boldsymbol{v}}_{\mathrm{f}}$, and $\widetilde{\psi}_{\mathrm{f}}$. Discretizing Eqs. (3.1), (3.2) and (3.3), weighting by appropriate test functions, and then integrating by parts over a cell yields the local weak form of the ALE Navier-Stokes equations defined over a cell. The full derivation is omitted here (See [3, 4]), but the resultant HDG ALE Navier-Stokes fluid problem is:

Problem 1 (Fluid sub-problem)**.**
Find $\{\mathbf{L}_{\mathrm{f}}^{\mathrm{h}},\mathbf{v}_{\mathrm{f}}^{\mathrm{h}},p_{\mathrm{f}}^{\mathrm{h}},\boldsymbol{v}_{\mathrm{f}}^{\mathrm{h}},\psi_{\mathrm{f}}^{\mathrm{h}}\}\in\boldsymbol{\mathcal{L}}_{\mathrm{f}}^{\mathrm{h}}\times\boldsymbol{V}_{\mathrm{f}}^{\mathrm{h}}\times\mathcal{P}_{\mathrm{f}}^{\mathrm{h}}\times\boldsymbol{\mathcal{V}}_{\mathrm{f}}^{\mathrm{h}}\times\Psi_{\mathrm{f}}^{\mathrm{h}}$ such that

$$
\begin{aligned}
&\left(\widetilde{\mathbf{v}}_{\mathrm{f}},\rho_{\mathrm{f}}J_{\mathrm{m}}\frac{\partial\mathbf{v}_{\mathrm{f}}^{\mathrm{h}}}{\partial t}\right)_{K_{\mathrm{f}}}+\left(\widetilde{\mathbf{v}}_{\mathrm{f}},\rho_{\mathrm{f}}J_{\mathrm{m}}\mathbf{L}_{\mathrm{f}}^{\mathrm{h}}\left[\mathbf{v}_{\mathrm{f}}^{\mathrm{h}}-\mathbf{v}_{\mathrm{m}}^{\mathrm{h}}\right]\right)_{K_{\mathrm{f}}}+\left(\widetilde{\mathbf{v}}_{\mathrm{f}},J_{\mathrm{m}}\mathbf{F}_{\mathrm{m}}^{-\mathsf{T}}\left[\mathrm{Grad}\,p_{\mathrm{f}}^{k}\right]\right)_{K_{\mathrm{f}}}\\
&\qquad+\left(\mathrm{Grad}\,\widetilde{\mathbf{v}}_{\mathrm{f}},\mu_{\mathrm{f}}J_{\mathrm{m}}\mathbf{L}_{\mathrm{f}}^{\mathrm{h}}\mathbf{F}_{\mathrm{m}}^{-\mathsf{T}}\right)_{K_{\mathrm{f}}}+\left\langle\widetilde{\mathbf{v}}_{\mathrm{f}},\widehat{\mathbf{T}}[\mathbf{n}]_{\mathrm{f}}^{*}\right\rangle_{\partial K_{\mathrm{f}}}=(\widetilde{\mathbf{v}}_{\mathrm{f}},J_{\mathrm{m}}\mathbf{f}_{\mathrm{f}})_{K_{\mathrm{f}}},\\
&\left(\widetilde{\mathbf{L}}_{\mathrm{f}},J_{\mathrm{m}}\mathbf{L}_{\mathrm{f}}^{\mathrm{h}}\right)_{K_{\mathrm{f}}}-\left(\widetilde{\mathbf{L}}_{\mathrm{f}},J_{\mathrm{m}}\mathrm{Grad}\,\mathbf{v}_{\mathrm{f}}^{\mathrm{h}}\mathbf{F}_{\mathrm{m}}^{-1}\right)_{K_{\mathrm{f}}}+\left\langle\widetilde{\mathbf{L}}_{\mathrm{f}}\mathbf{F}_{\mathrm{m}}^{-\mathsf{T}}[\mathbf{n}_{\mathrm{f}}],J_{\mathrm{m}}\left(\mathbf{v}_{\mathrm{f}}^{\mathrm{h}}-\boldsymbol{v}_{\mathrm{f}}^{\mathrm{h}}\right)\right\rangle_{\partial K_{\mathrm{f}}}=0,\\
&-\left(\mathbf{F}_{\mathrm{m}}^{-\mathsf{T}}\left[\mathrm{Grad}\,\widetilde{p}_{\mathrm{f}}^{k}\right],J_{\mathrm{m}}\mathbf{v}_{\mathrm{f}}^{\mathrm{h}}\right)_{K_{\mathrm{f}}}+\left\langle\mathbf{F}_{\mathrm{m}}^{-\mathsf{T}}[\mathbf{n}_{\mathrm{f}}]\widetilde{p}_{\mathrm{f}}^{k},J_{\mathrm{m}}\boldsymbol{v}_{\mathrm{f}}^{\mathrm{h}}\right\rangle_{\partial K_{\mathrm{f}}}=0,\\
&\left\langle\widetilde{\boldsymbol{v}}_{\mathrm{f}},\widehat{\mathbf{T}}[\mathbf{n}]_{\mathrm{f}}\right\rangle_{\partial\mathcal{T}_{\mathrm{f}}^{\mathrm{h}}\backslash\Gamma_{\mathrm{FSI}}}+\left\langle\widetilde{\boldsymbol{v}}_{\mathrm{f}},\widehat{\mathbf{T}}[\mathbf{n}]_{\mathrm{f}}+\widehat{\mathbf{T}}[\mathbf{n}]_{\mathrm{s}}\right\rangle_{\Gamma_{\mathrm{FSI}}}+\left\langle\widetilde{\boldsymbol{v}}_{\mathrm{f}},\mathbf{S}_{\mathrm{f}}\left(\boldsymbol{v}_{\mathrm{f}}^{\mathrm{h}}-\boldsymbol{v}_{\mathrm{s}}^{\mathrm{h}}\right)\right\rangle_{\Gamma_{\mathrm{FSI}}}=\langle\widetilde{\boldsymbol{v}}_{\mathrm{f}},J_{\mathrm{m}}\mathbf{g}_{\mathrm{N_f}}\rangle_{\Gamma_{\mathrm{N}}},\\
&\left\langle\widetilde{\psi}_{\mathrm{f}},J_{\mathrm{m}}\mathbf{F}_{\mathrm{m}}^{-\mathsf{T}}[\mathbf{n}_{\mathrm{f}}]\cdot\boldsymbol{v}_{\mathrm{f}}^{\mathrm{h}}\right\rangle_{\partial\mathcal{T}_{\mathrm{f}}^{\mathrm{h}}}=0,\\
&(\widetilde{p}_{\mathrm{f}}^{0},J_{\mathrm{m}}p_{\mathrm{f}}^{0})_{\mathcal{T}_{\mathrm{f}}^{\mathrm{h}}}=0,\\
&\forall\{\widetilde{\mathbf{L}}_{\mathrm{f}},\widetilde{\mathbf{v}}_{\mathrm{f}},\widetilde{p}_{\mathrm{f}},\widetilde{\boldsymbol{v}}_{\mathrm{f}},\widetilde{\psi}_{\mathrm{f}}\}\in\boldsymbol{\mathcal{L}}_{\mathrm{f}}^{\mathrm{h}}\times\boldsymbol{V}_{\mathrm{f}}^{\mathrm{h}}\times\mathcal{P}_{\mathrm{f}}^{\mathrm{h}}\times\widetilde{\boldsymbol{\mathcal{V}}}_{\mathrm{f}}\times\Psi_{\mathrm{f}}^{\mathrm{h}},
\end{aligned}
$$

where

$$
\begin{aligned}
&p_{\mathrm{f}}^{0}+p_{\mathrm{f}}^{k}=p_{\mathrm{f}}^{\mathrm{h}},\\
&\widehat{\mathbf{T}}[\mathbf{n}]_{\mathrm{f}}^{*}:=-\mu_{\mathrm{f}}J_{\mathrm{m}}\mathbf{L}_{\mathrm{f}}^{\mathrm{h}}\mathbf{F}_{\mathrm{m}}^{-\mathsf{T}}[\mathbf{n}_{\mathrm{f}}]+\mathbf{S}_{\mathrm{f}}\left(\mathbf{v}_{\mathrm{f}}^{\mathrm{h}}-\boldsymbol{v}_{\mathrm{f}}^{\mathrm{h}}\right),\\
&\widehat{\mathbf{T}}[\mathbf{n}]_{\mathrm{f}}:=J_{\mathrm{m}}\left[-\mu_{\mathrm{f}}\mathbf{L}_{\mathrm{f}}^{\mathrm{h}}+\left(p_{\mathrm{f}}^{k}+\psi_{\mathrm{f}}^{\mathrm{h}}\right)\mathbf{I}\right]\mathbf{F}_{\mathrm{m}}^{-\mathsf{T}}[\mathbf{n}_{\mathrm{f}}]+\mathbf{S}_{\mathrm{f}}\left(\mathbf{v}_{\mathrm{f}}^{\mathrm{h}}-\boldsymbol{v}_{\mathrm{f}}^{\mathrm{h}}\right),\\
&\mathbf{S}_{\mathrm{f}}:=\left(\frac{\mu_{\mathrm{f}}}{l_{\mathrm{f}}}+\rho_{\mathrm{f}}\left|\mathbf{v}_{\mathrm{f}}^{\mathrm{h}}\right|_{\mathrm{L2}}\right)\mathbf{I}.
\end{aligned}
$$

It is worth noting that the pressure was decomposed by

$$
p_{\mathrm{f}}^{\mathrm{h}}:=p_{\mathrm{f}}^{0}+p_{\mathrm{f}}^{\mathrm{k}},\quad\text{s.t.}\quad\mathrm{Grad}\,p_{\mathrm{f}}^{0}=0,\quad\&\quad\int_{\mathrm{V}}p_{\mathrm{f}}^{\mathrm{k}}\mathrm{dV}=0,\tag{3.23}
$$

where p_{f}^{0} and $p_{\mathrm{f}}^{\mathrm{k}}$ are from the following spaces:

$$
\begin{aligned}
&Q^{0}:=\left\{p_{\mathrm{f}}^{0}\in L^{2}\left(\mathcal{T}^{\mathrm{h}}\right):\ p_{\mathrm{f}}^{0}\big|_{K}\in P_{0}(K),\quad\forall K\in\mathcal{T}^{\mathrm{h}}\right\},\\
&Q^{\mathrm{k}}:=Q^{\mathrm{h}}\backslash Q^{0}.
\end{aligned}\tag{3.24}
$$

Also, to minimize the number of global DOFs, approximations of the velocity-gradient trace and pressure trace from the traction $\widehat{\mathbf{T}}$ were defined in terms of the other variables and a stabilization parameter $\mathbf{S}$ and a characteristic length scale l. This is also done for the solid and mesh formulations.

3.4.2 Solid

The solid governing equations are where the major differences in formulation occur. Below, the two-hybrid-field formulation from [3,4] is reproduced, followed by the new one-hybrid-field formulation. The discretized primary variables for solid formulation are the Green-St. Venant strain $\mathbf{E}_{\rm s}^{\rm h}$, the displacement $\mathbf{u}_{\rm s}^{\rm h}$, the velocity $\mathbf{v}_{\rm s}^{\rm h}$, the trace of the displacement over the element faces $\boldsymbol{\mu}_{\rm s}^{\rm h}$ (only in the old two-hybrid-field formulation), and the trace of the velocity over the element faces $\boldsymbol{v}_{\rm s}^{\rm h}$. Each has an associated test function: $\widetilde{\mathbf{E}}_{\rm s}$, $\widetilde{\mathbf{u}}_{\rm s}$, $\widetilde{\mathbf{v}}_{\rm s}$, $\widetilde{\boldsymbol{\mu}}_{\rm s}$, and $\widetilde{\boldsymbol{v}}_{\rm s}$. For the two-hybrid-field formulation, an added constraint is necessary that specifies that the global displacement equals the local displacement on the element faces. This constraint is *not* necessary in the new one-hybrid-field formulation.

Problem 2 (Two-hybrid-field solid sub-problem)**.**
Find $\{\mathbf{u}_{\rm s}^{\rm h},\mathbf{v}_{\rm s}^{\rm h},\mathbf{E}_{\rm s}^{\rm h},\boldsymbol{\mu}_{\rm s}^{\rm h},\boldsymbol{v}_{\rm s}^{\rm h}\}\in\boldsymbol{U}_{\rm s}^{\rm h}\times\boldsymbol{V}_{\rm s}^{\rm h}\times\boldsymbol{\mathcal{E}}_{\rm s}^{\rm h}\times\boldsymbol{M}_{\rm s}^{\rm h}\times\boldsymbol{\mathcal{V}}_{\rm s}^{\rm h}$, such that

$$
\begin{aligned}
&\left(\widetilde{\mathbf{v}}_{\rm s},\rho\frac{\partial\mathbf{v}_{\rm s}^{\rm h}}{\partial t}\right)_{K_{\rm s}}+\left(\mathrm{Grad}\widetilde{\mathbf{v}}_{\rm s},\mathbf{F}_{\rm s}\mathbb{C}_{\rm s}\left(\mathbf{E}_{\rm s}^{\rm h}\right)\right)_{K_{\rm s}}+\left\langle\widetilde{\mathbf{v}}_{\rm s},\widehat{\mathbf{T}}[\mathbf{n}]_{\rm s}\right\rangle_{\partial K_{\rm s}}=(\widetilde{\mathbf{v}}_{\rm s},\mathbf{f}_{\rm s})_{K_{\rm s}},\\
&\left(\widetilde{\mathbf{E}}_{\rm s},\mathbf{E}_{\rm s}^{\rm h}\right)_{K_{\rm s}}-\left(\mathrm{Sym}(\widetilde{\mathbf{E}})_{\rm s},\mathrm{Grad}\,\mathbf{u}_{\rm s}^{\rm h}\right)_{K_{\rm s}}-\left(\tfrac{1}{2}\widetilde{\mathbf{E}}_{\rm s},\left(\mathrm{Grad}\,\mathbf{u}_{\rm s}^{\rm h}\right)^{\mathsf{T}}\mathrm{Grad}\,\mathbf{u}_{\rm s}^{\rm h}\right)_{K_{\rm s}}\\
&\qquad+\left\langle\mathrm{Sym}(\widetilde{\mathbf{E}})_{\rm s}\mathbf{n},\left(\mathbf{u}_{\rm s}^{\rm h}-\boldsymbol{\mu}_{\rm s}^{\rm h}\right)\right\rangle_{\partial K_{\rm s}}=0,\\
&\left(\widetilde{\mathbf{u}}_{\rm s},\frac{\partial\mathbf{u}_{\rm s}^{\rm h}}{\partial t}\right)_{K_{\rm s}}-\left(\widetilde{\mathbf{u}}_{\rm s},\mathbf{v}_{\rm s}^{\rm h}\right)_{K_{\rm s}}=0,\\
&\left\langle\widetilde{\boldsymbol{\mu}}_{\rm s},\mathbf{u}_{\rm s}^{\rm h}\right\rangle_{\partial K_{\rm s}}-\left\langle\widetilde{\boldsymbol{\mu}}_{\rm s},\boldsymbol{\mu}_{\rm s}^{\rm h}\right\rangle_{\partial K_{\rm s}}=0,\\
&\left\langle\widetilde{\boldsymbol{v}}_{\rm s},\widehat{\mathbf{T}}[\mathbf{n}]_{\rm s}\right\rangle_{\partial\mathcal{T}_{\rm s}^{\rm h}\setminus\Gamma_{\rm FSI}}+\left\langle\widetilde{\boldsymbol{v}}_{\rm s},\widehat{\mathbf{T}}[\mathbf{n}]_{\rm s}+\widehat{\mathbf{T}}[\mathbf{n}]_{\rm f}\right\rangle_{\Gamma_{\rm FSI}}+\left\langle\widetilde{\boldsymbol{v}}_{\rm s},\mathbf{S}_{\rm s}\left(\boldsymbol{v}_{\rm s}^{\rm h}-\boldsymbol{v}_{\rm f}^{\rm h}\right)\right\rangle_{\Gamma_{\rm FSI}}=\langle\widetilde{\boldsymbol{v}}_{\rm s},\mathbf{g}_{\rm N_s}\rangle_{\Gamma_{\rm N_s}},\\
&\forall\{\widetilde{\mathbf{u}}_{\rm s},\widetilde{\mathbf{v}}_{\rm s},\widetilde{\mathbf{E}}_{\rm s},\widetilde{\boldsymbol{\mu}}_{\rm s},\widetilde{\boldsymbol{v}}_{\rm s}\}\in\boldsymbol{U}^{\rm h}\times\boldsymbol{V}_{\rm s}^{\rm h}\times\boldsymbol{\mathcal{E}}_{\rm s}^{\rm h}\times\widetilde{\boldsymbol{M}}_{\rm s}\times\boldsymbol{\mathcal{V}}_{\rm s}^{\rm h},
\end{aligned}
$$

where

$$
\begin{aligned}
&\mathbf{F}_{\rm s}=\mathbf{I}+\mathrm{Grad}\,\mathbf{u}_{\rm s}^{\rm h},\\
&\widehat{\mathbf{T}}[\mathbf{n}]_{\rm s}:=-\left[\mathbf{F}_{\rm s}\mathbb{C}_{\rm s}\left(\mathbf{E}_{\rm s}^{\rm h}\right)\right]\mathbf{n}_{\rm s}+\mathbf{S}_{\rm s}\left(\mathbf{v}_{\rm s}^{\rm h}-\boldsymbol{v}_{\rm s}^{\rm h}\right),\\
&\mathbf{S}_{\rm s}:=\frac{\mu_{\rm s}}{l_{\rm s}}\mathbf{I}.
\end{aligned}
$$

Problem 3 (One-hybrid-field solid sub-problem)**.**
Find $\{\mathbf{u}_{\mathrm{s}}^{\mathrm{h}},\mathbf{v}_{\mathrm{s}}^{\mathrm{h}},\mathbf{E}_{\mathrm{s}}^{\mathrm{h}},\boldsymbol{v}_{\mathrm{s}}^{\mathrm{h}}\}\in\boldsymbol{U}_{\mathrm{s}}^{\mathrm{h}}\times\boldsymbol{V}_{\mathrm{s}}^{\mathrm{h}}\times\boldsymbol{\mathcal{E}}_{\mathrm{s}}^{\mathrm{h}}\times\boldsymbol{\mathcal{V}}_{\mathrm{s}}^{\mathrm{h}}$, such that

$$
\begin{aligned}
&\left(\widetilde{\mathbf{v}}_{\mathrm{s}},\rho\frac{\partial\mathbf{v}_{\mathrm{s}}^{\mathrm{h}}}{\partial t}\right)_{K_{\mathrm{s}}}+\left(\mathrm{Grad}\,\widetilde{\mathbf{v}}_{\mathrm{s}},\mathbf{F}_{\mathrm{s}}\mathbb{C}_{\mathrm{s}}\left(\mathbf{E}_{\mathrm{s}}^{\mathrm{h}}\right)\right)_{K_{\mathrm{s}}}+\left\langle\widetilde{\mathbf{v}}_{\mathrm{s}},\widehat{\mathbf{T}}[\mathbf{n}]_{\mathrm{s}}\right\rangle_{\partial K_{\mathrm{s}}}=(\widetilde{\mathbf{v}}_{\mathrm{s}},\mathbf{f}_{\mathrm{s}})_{K_{\mathrm{s}}},\\
&\left(\widetilde{\mathbf{E}}_{\mathrm{s}},\frac{\partial\mathbf{E}_{\mathrm{s}}^{\mathrm{h}}}{\partial t}\right)_{K_{\mathrm{s}}}-\left(\mathrm{Sym}(\widetilde{\mathbf{E}})_{\mathrm{s}},\mathrm{Grad}\,\mathbf{v}_{\mathrm{s}}^{\mathrm{h}}\right)_{K_{\mathrm{s}}}-\left(\tfrac{1}{2}\widetilde{\mathbf{E}}_{\mathrm{s}},\left(\mathrm{Grad}\,\mathbf{v}_{\mathrm{s}}^{\mathrm{h}}\right)^{\mathsf{T}}\mathrm{Grad}\,\mathbf{u}_{\mathrm{s}}^{\mathrm{h}}\right)_{K_{\mathrm{s}}}\\
&\qquad\qquad-\left(\tfrac{1}{2}\widetilde{\mathbf{E}}_{\mathrm{s}},\left(\mathrm{Grad}\,\mathbf{u}_{\mathrm{s}}^{\mathrm{h}}\right)^{\mathsf{T}}\mathrm{Grad}\,\mathbf{v}_{\mathrm{s}}^{\mathrm{h}}\right)_{K_{\mathrm{s}}}+\left\langle\mathrm{Sym}(\widetilde{\mathbf{E}})_{\mathrm{s}}\mathbf{n},\left(\mathbf{v}_{\mathrm{s}}^{\mathrm{h}}-\boldsymbol{v}_{\mathrm{s}}^{\mathrm{h}}\right)\right\rangle_{\partial K_{\mathrm{s}}}=0,\\
&\left(\widetilde{\mathbf{u}}_{\mathrm{s}},\frac{\partial\mathbf{u}_{\mathrm{s}}^{\mathrm{h}}}{\partial t}\right)_{K_{\mathrm{s}}}-\left(\widetilde{\mathbf{u}}_{\mathrm{s}},\mathbf{v}_{\mathrm{s}}^{\mathrm{h}}\right)_{K_{\mathrm{s}}}=0,\\
&\left\langle\widetilde{\boldsymbol{v}}_{\mathrm{s}},\widehat{\mathbf{T}}[\mathbf{n}]_{\mathrm{s}}\right\rangle_{\partial\mathcal{T}_{\mathrm{s}}^{\mathrm{h}}\backslash\Gamma_{\mathrm{FSI}}}+\left\langle\widetilde{\boldsymbol{v}}_{\mathrm{s}},\widehat{\mathbf{T}}[\mathbf{n}]_{\mathrm{s}}+\widehat{\mathbf{T}}[\mathbf{n}]_{\mathrm{f}}\right\rangle_{\Gamma_{\mathrm{FSI}}}+\left\langle\widetilde{\boldsymbol{v}}_{\mathrm{s}},\mathbf{S}_{\mathrm{s}}\left(\boldsymbol{v}_{\mathrm{s}}^{\mathrm{h}}-\boldsymbol{v}_{\mathrm{f}}^{\mathrm{h}}\right)\right\rangle_{\Gamma_{\mathrm{FSI}}}=\langle\widetilde{\boldsymbol{v}}_{\mathrm{s}},\mathbf{g}_{\mathrm{N_s}}\rangle_{\Gamma_{\mathrm{N_s}}},\\
&\forall\{\widetilde{\mathbf{u}}_{\mathrm{s}},\widetilde{\mathbf{v}}_{\mathrm{s}},\widetilde{\mathbf{E}}_{\mathrm{s}},\widetilde{\boldsymbol{v}}_{\mathrm{s}}\}\in\boldsymbol{U}^{\mathrm{h}}\times\boldsymbol{V}_{\mathrm{s}}^{\mathrm{h}}\times\boldsymbol{\mathcal{E}}_{\mathrm{s}}^{\mathrm{h}}\times\boldsymbol{\mathcal{V}}_{\mathrm{s}}^{\mathrm{h}},
\end{aligned}
$$

where

$$
\begin{aligned}
&\mathbf{F}_{\mathrm{s}}=\mathbf{I}+\mathrm{Grad}\,\mathbf{u}_{\mathrm{s}}^{\mathrm{h}},\\
&\widehat{\mathbf{T}}[\mathbf{n}]_{\mathrm{s}}:=-\left[\mathbf{F}_{\mathrm{s}}\mathbb{C}_{\mathrm{s}}\left(\mathbf{E}_{\mathrm{s}}^{\mathrm{h}}\right)\right]\mathbf{n}_{\mathrm{s}}+\mathbf{S}_{\mathrm{s}}\left(\mathbf{v}_{\mathrm{s}}^{\mathrm{h}}-\boldsymbol{v}_{\mathrm{s}}^{\mathrm{h}}\right),\\
&\mathbf{S}_{\mathrm{s}}:=\frac{\mu_{\mathrm{s}}}{l_{\mathrm{s}}}\mathbf{I}.
\end{aligned}
$$

3.4.3 Mesh

Finally, the mesh governing equations are presented in almost exactly the same form as they were in [3,4], with the exception of the change to the solid-mesh displacement condition from Eq. (3.20) and the restricted function spaces from Eq. (3.22). The discretized primary variables for mesh formulation are the deformation-gradient $\mathbf{F}_{\mathrm{m}}^{\mathrm{h}}$, the displacement $\mathbf{u}_{\mathrm{m}}^{\mathrm{h}}$, and the trace of the displacement over the element faces $\boldsymbol{\mu}_{\mathrm{m}}^{\mathrm{h}}$. Each has an associated test function: $\widetilde{\mathbf{F}}_{\mathrm{m}}$, $\widetilde{\mathbf{u}}_{\mathrm{m}}$, and $\widetilde{\boldsymbol{\mu}}_{\mathrm{m}}$.

Problem 4 (Mesh sub-problem)**.**
Find $\{\mathbf{u}_{\mathrm{m}}^{\mathrm{h}},\mathbf{F}_{\mathrm{m}}^{\mathrm{h}},\boldsymbol{\mu}_{\mathrm{m}}^{\mathrm{h}}\}\in\boldsymbol{U}_{\mathrm{m}}^{1}\times\boldsymbol{\mathcal{F}}_{\mathrm{m}}^{1}\times\boldsymbol{M}_{\mathrm{m}}^{1}$ such that

$$
\begin{aligned}
&\left(\mathrm{Grad}\,\widetilde{\mathbf{u}}_{\mathrm{m}},\mathbb{C}_{\mathrm{m}}\left(\mathbf{F}_{\mathrm{m}}^{\mathrm{h}}\right)\right)_{K}-\left\langle\widetilde{\mathbf{u}}_{\mathrm{m}},\widehat{\mathbf{T}}[\mathbf{n}]_{\mathrm{m}}\right\rangle_{\partial K}=(\mathrm{Grad}\,\widetilde{\mathbf{u}}_{\mathrm{m}},\mathbb{C}_{\mathrm{m}}(\mathbf{I}))_{K}-\langle\widetilde{\mathbf{u}}_{\mathrm{m}},\mathbb{C}_{\mathrm{m}}(\mathbf{I})\mathbf{n}_{\mathrm{m}}\rangle_{\partial K}+(\widetilde{\mathbf{u}}_{\mathrm{m}},\mathbf{f})_{K},\\
&\left(\widetilde{\mathbf{F}}_{\mathrm{m}},\mathbf{F}_{\mathrm{m}}^{\mathrm{h}}\right)_{K}-\left(\widetilde{\mathbf{F}}_{\mathrm{m}},\mathrm{Grad}\,\mathbf{u}_{\mathrm{m}}^{\mathrm{h}}\right)_{K}+\left\langle\widetilde{\mathbf{F}}_{\mathrm{m}}\mathbf{n}_{\mathrm{m}},\left(\mathbf{u}_{\mathrm{m}}^{\mathrm{h}}-\boldsymbol{\mu}_{\mathrm{m}}^{\mathrm{h}}\right)\right\rangle_{\partial K}=\left(\widetilde{\mathbf{F}}_{\mathrm{m}},\mathbf{I}\right)_{K},\\
&\left\langle\widetilde{\boldsymbol{\mu}}_{\mathrm{m}},\widehat{\mathbf{T}}[\mathbf{n}]_{\mathrm{m}}\right\rangle_{\partial\mathcal{T}_{\mathrm{m}}^{\mathrm{h}}\backslash\Gamma_{\mathrm{FSI}}}+\left\langle\widetilde{\boldsymbol{\mu}}_{\mathrm{m}},\boldsymbol{\mu}_{\mathrm{m}}^{\mathrm{h}}-\mathbf{u}_{\mathrm{s}}^{\mathrm{h}}\right\rangle_{\Gamma_{\mathrm{FSI}}}=\langle\widetilde{\boldsymbol{\mu}}_{\mathrm{m}},\mathbb{C}_{\mathrm{m}}(\mathbf{I})\mathbf{n}_{\mathrm{m}}\rangle_{\partial\mathcal{T}_{\mathrm{m}}^{\mathrm{h}}\backslash\Gamma_{\mathrm{FSI}}}+\langle\widetilde{\boldsymbol{\mu}}_{\mathrm{m}},\mathbf{g}_{\mathrm{N}}\rangle_{\partial\Omega_{\mathrm{N}}},\\
&\forall\{\widetilde{\mathbf{u}}_{\mathrm{m}},\widetilde{\mathbf{F}}_{\mathrm{m}},\widetilde{\boldsymbol{\mu}}_{\mathrm{m}}\}\in\boldsymbol{U}_{\mathrm{m}}^{1}\times\boldsymbol{\mathcal{F}}_{\mathrm{m}}^{1}\times\widetilde{\boldsymbol{M}}_{\mathrm{m}}^{1},
\end{aligned}
$$

where

$$\widehat{\mathbf{T}}[\mathbf{n}]_{\mathrm{m}} := \mathbb{C}_{\mathrm{m}}\left(\mathbf{F}_{\mathrm{m}}^{\mathrm{h}}\right)\mathbf{n}_{\mathrm{m}} - \mathbf{S}_{\mathrm{m}}\left(\mathbf{u}_{\mathrm{m}}^{\mathrm{h}} - \boldsymbol{\mu}_{\mathrm{m}}^{\mathrm{h}}\right),$$
$$\mathbf{S}_{\mathrm{m}} := \frac{\mu_{\mathrm{m}}}{l_{\mathrm{m}}}\mathbf{I}.$$

3.5 Monolithic fluid-structure interaction

The global FSI problem is a direct sum of Problems 1, 3, and 4 with coupling conditions.

Problem 5 (Global FSI problem)**.**
Find $\{\mathbf{L}_{\mathrm{f}}^{\mathrm{h}}, \mathbf{v}_{\mathrm{f}}^{\mathrm{h}}, p_{\mathrm{f}}^{\mathrm{h}}, \boldsymbol{v}_{\mathrm{f}}^{\mathrm{h}}, \psi_{\mathrm{f}}^{\mathrm{h}}\} \in \boldsymbol{\mathcal{L}}_{\mathrm{f}}^{\mathrm{h}} \times \boldsymbol{V}_{\mathrm{f}}^{\mathrm{h}} \times \mathcal{P}_{\mathrm{f}}^{\mathrm{h}} \times \boldsymbol{\mathcal{V}}_{\mathrm{f}}^{\mathrm{h}} \times \Psi_{\mathrm{f}}^{\mathrm{h}}$, $\{\mathbf{u}_{\mathrm{s}}^{\mathrm{h}}, \mathbf{v}_{\mathrm{s}}^{\mathrm{h}}, \mathbf{E}_{\mathrm{s}}^{\mathrm{h}}, \boldsymbol{v}_{\mathrm{s}}^{\mathrm{h}}\} \in \boldsymbol{U}_{\mathrm{s}}^{\mathrm{h}} \times \boldsymbol{V}_{\mathrm{s}}^{\mathrm{h}} \times \boldsymbol{\mathcal{E}}_{\mathrm{s}}^{\mathrm{h}} \times \boldsymbol{\mathcal{V}}_{\mathrm{s}}^{\mathrm{h}}$, and $\{\mathbf{u}_{\mathrm{m}}^{\mathrm{h}}, \mathbf{F}_{\mathrm{m}}^{\mathrm{h}}, \boldsymbol{\mu}_{\mathrm{m}}^{\mathrm{h}}\} \in \boldsymbol{U}_{\mathrm{m}}^{1} \times \boldsymbol{\mathcal{F}}_{\mathrm{m}}^{1} \times \boldsymbol{M}_{\mathrm{m}}^{1}$ such that Problems 1, 3, and 4 are simultaneously satisfied.

The globally defined system in Problem 5 is a fully coupled nonlinear system of equations. The Newton-Raphson procedure [24] is employed to solve these nonlinear equations.

4 Numerical results

Code-to-code comparison is considered against the benchmark given in [23] by Turek and Hron, with domain detailed in Fig. 1. All dimensions and properties used are from [23] for case "FSI2" and are reproduced in Table 1. The FSI benchmark simulates two-dimensional incompressible channel flow around a rigid cylinder with an attached nonlinearly elastic flag. The wake shed from the cylinder produces oscillations in the flag that self-excite and eventually reach a stationary oscillatory state. The initial conditions are zero

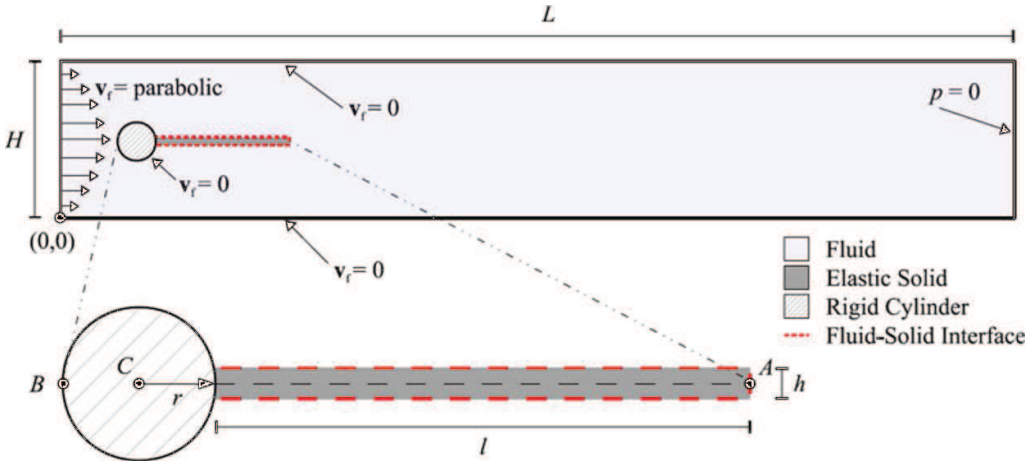

Figure 1: The domain used for the FSI benchmark proposed by [23]. The benchmark simulates two-dimensional channel flow over a rigid cylinder with a flexible flag attached.

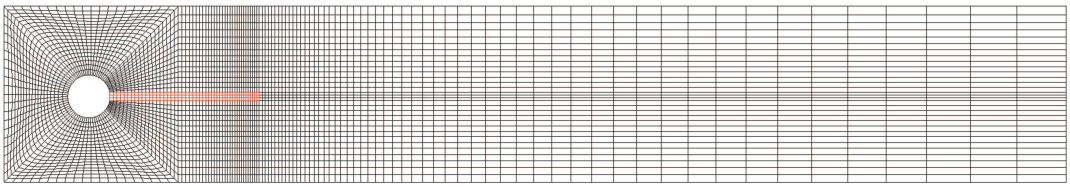

Figure 2: A diagram of the (undeformed) mesh used for the HDG FSI simulation of the Turek and Hron benchmark [23]. There are 4217 fluid cells, indicated in black, and 147 solid cells, indicated in red.

Table 1: Turek and Hron [23] benchmark domain dimensions and material properties.

Parameter	Symbol	Value [m]	Property	Value
Channel length	L	2.5	ρ_s $[\frac{kg}{m^3}]$	10000
Channel height	H	0.41	ν_s	0.4
Cylinder center	C	(0.2, 0.2)	E_s $[\text{E6}\,\frac{kg}{ms^2}]$	5.6
Cylinder radius	r	0.05	ρ_f $[\frac{kg}{m^3}]$	1000
Flag length	l	0.35	μ_f $[\frac{kg}{ms}]$	1
Flag height	h	0.02	$\bar{U}$ $[\frac{m}{s}]$	1
Reference point	A	(0.6, 0.2)		
Reference point	B	(0.15, 0.2)	$\mathbf{v}_f\|_{in}$ $[\frac{m}{s}]$	$1.5\bar{U}\frac{y(H-y)}{(H/2)^2}$

everywhere and the inlet velocity smoothly increases to $\mathbf{v}_f|_{in}$ over the first two seconds. After the first two seconds, the inlet velocity is constant. The top and bottom boundaries of the channel are subject to the no-slip condition, as is the perimeter of the rigid cylinder. The flag, attached to the cylinder, is allowed to move freely with the fluid flow, subject to the interface conditions specified in Eqs. (3.18), (3.19), and (3.20). The BDF2 timestepping method is used with a timestep size $\Delta t = 0.0025$ for all of the results in this section. The HDG FSI model and subproblems were implemented utilizing the deal.II finite element library [25, 26]. The mesh used for all the results in this section is presented in Fig. 2, which contains 4364 cells combined between the solid and fluid. Turek and Hron provided tip displacement data for point A, from Fig. 1, and the drag and lift calculated about the perimeter of the cylinder and attached flag. Fig. 3 contains plots for each of these metrics, with a comparison between the results from [3,4], labeled "Old HDG FSI", the results from the reduced DOF formulation presented in this work, labeled "Reduced DOF HDG FSI", and the results from Turek and Hron's benchmark [23], labeled "Turek FSI". As can be seen in the figure, the results from [3,4] and this work are indistinguishable from each other and, while there remains some discrepancy[‡] between both sets of

[‡]We expect the discrepancy between the HDG FSI2 results and the Turek and Hron FSI2 results is caused by the choice of stabilization tensor $\mathbf{S}$ for the system, as is discussed in more detail in [3,4]. HDG stabilization for multi-physics systems is mostly unexplored in the literature and currently poorly understood. It remains an important area of future work.

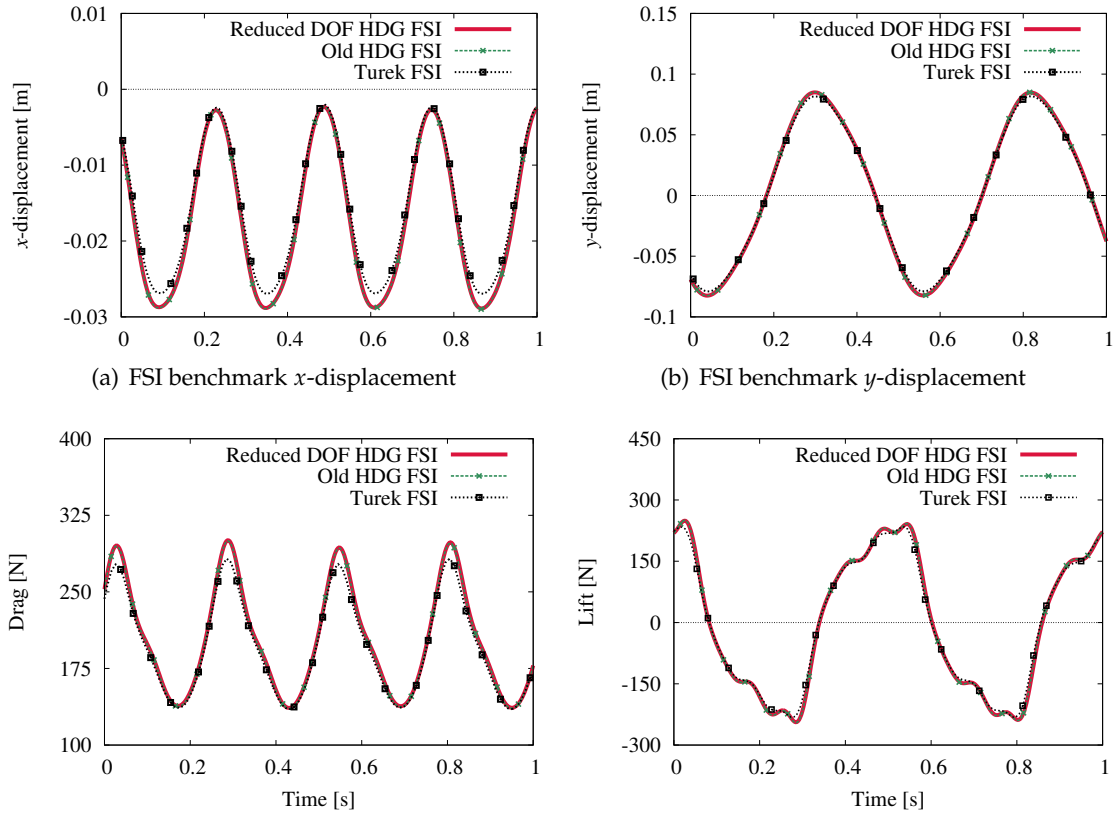

(a) FSI benchmark x-displacement

(b) FSI benchmark y-displacement

(c) FSI benchmark drag

(d) FSI benchmark lift

Figure 3: Comparison of x- and y-displacement at point A from Fig. 1, and of drag and lift calculated about the perimeter of the cylinder and flag from Fig. 1, between Turek and Hron's FSI benchmark [23] and HDG results, over a period of stationary oscillation. The HDG results were calculated using Q2 elements and the BDF2 timestepping method. The points indicated on the data in these plots hold no physical significance and are only present to distinguish the data when they overlap.

HDG results and the Turek and Hron results, the important fact is that the new reduced DOF formulation documented in this work did not negatively impact the accuracy of the solution at all compared to the previous formulation, while substantially decreasing number of DOFs required for the calculation.

Table 2 lists the number of DOFs required by both the old and new HDG FSI formulations for the presented FSI2 results, as well as the percent reduction of DOFs with the formulation from this work over the old formulation. There is a total global DOF reduction of 17% and total local DOF reduction of 25%. This directly translates to improved computational efficiency, especially due to the global DOF reduction. It is worth noting that the solid global DOF reduction is 50%, so a problem with a larger solid domain relative to the fluid domain would experience even greater improvement in computational efficiency. Additionally, the case presented uses only quadratic tensor-product polyno-

Table 2: The number of DOFs for the solid domain and the fluid domain, for both the formulation from [3, 4] and this work's. The fluid and mesh DOFs are both included in the fluid domain. The third set of columns shows the percent DOF reduction with the formulation presented in this work versus that from [3, 4].

	Old HDG FSI		Reduced DOF HDG FSI		Percent DOF reduction	
	Global DOFs	Local DOFs	Global DOFs	Local DOFs	Global DOFs	Local DOFs
Fluid	108125	493389	90807	366879	16%	26%
Solid	4152	10584	2076	10584	50%	0%
Total	112277	503973	92883	377463	17%	25%

mial elements (Q2-elements). For higher order elements, there will be a substantially increased DOF reduction (both locally and globally) due to the restriction of the mesh function spaces to only linear polynomials, as shown in Appendix A. Also, the fluid domain values from Table 2 directly agree with the arbitrary values from Table 4 for $d=k=2$.

In performing this numerical analysis, an additional, unexpected, benefit to the restricted mesh function spaces was discovered. The linear function spaces produced higher quality meshes and increased the stability of the system under large deformations compared to the equal-order mesh formulation. Problems with moving domains, such as FSI with the ALE Navier-Stokes equations, often suffer from not maintaining high mesh quality over time. If a mesh's quality becomes so poor[§] that it contains a negative volume, linear algebra solvers will be unable to produce a solution, resulting in a failed simulation. In this work, for this specific benchmark, the mesh's material parameters are defined to make it radially less stiff outward from the tip of the flag. This disperses the mesh deformation throughout the mesh domain instead of localizing it about the FSI interface. With the linear mesh functions spaces cell quality was preserved at a higher level throughout the domain better than with the equal-order mesh function spaces.

4.1 Per-Element DOF-Reduction

The primary result from this work is the reduction in the DOFs per cell and face achieved while still maintaining the accuracy of the solution compared to the old method. The code-to-code comparison presented in the previous section demonstrates that the solution obtained by the new, less computationally expensive, method successfully predicts the Turek-Hron benchmark solution to the same accuracy as the old, more computationally expensive, method. In this section, a quantitative reduction in the number of DOFs per cell and cell face, for two and three dimensional elements, for polynomial orders k=1-10 are given.

Table 3 gives the number of DOFs for a fluid-ALE domain cell and cell face, computed by adapting the equations for the global number of unknowns given in Appendix A. In

[§]A poor quality mesh satisfies its boundary conditions but contains cells that are extremely distorted, such as cells with nearly parallel adjacent sides.

Table 3: Local DOFs for the fluid problem versus polynomial order and dimension. The new formulation results in a significant reduction in the number of DOFs.

Local DOFs Per Fluid Cell						
Dimension	2			3		
	OLD	NEW	Reduction	OLD	NEW	Reduction
Order (k)						
1	52	52	0.00 %	200	200	0.00%
2	117	87	25.64%	675	447	33.78%
3	208	136	34.62%	1600	928	42.00%
4	325	199	38.77%	3125	1721	44.93%
5	468	276	41.03%	5400	2904	46.22%
6	637	367	42.39%	8575	4555	46.88%
7	832	472	43.27%	12800	6752	47.25%
8	1053	591	43.87%	18225	9573	47.47%
9	1300	724	44.31%	25000	13096	47.62%
10	1573	871	44.63%	33275	17399	47.71%

Global DOFs Per Fluid Face						
Dimension	2			3		
	OLD	NEW	Reduction	OLD	NEW	Reduction
Order (k)						
1	8	8	0.00 %	24	24	0.00 %
2	12	10	16.67%	54	39	27.78%
3	16	12	25.00%	96	60	37.50%
4	20	14	30.00%	150	87	42.00%
5	24	16	33.33%	216	120	44.44%
6	28	18	35.71%	294	159	45.92%
7	32	20	37.50%	384	204	46.88%
8	36	22	38.89%	486	255	47.53%
9	40	24	40.00%	600	312	48.00%
10	44	26	40.91%	726	375	48.35%

each case, the number of DOFs is seen to reduce in both two and three dimensions as the finite element polynomial order k is increased. The effect of reformulating the problem is more pronounced in three dimensions then in two, indicating that more complex three dimensional applications stand to gain significantly improved efficiency by using the new formulation.

The solid domain (elasticity) formulation has no reduction in the number of local per-cell DOFs, but does see a 50% reduction in the number of global DOFs, simply by removing one the global fields in the new formulation presented in this work.

5 Conclusion

This work presents a hybridizable discontinuous Galerkin finite element formulation for fluid structure interaction with substantially improved computational efficiency, in terms of a significant reduction in the number of global and local DOFs per cell, compared to the original HDG FSI formulation developed by Sheldon et al. [3, 4]. The resulting linearized system is smaller and does not increase the number of non-zeros for retained DOFs. Furthermore, the stability and accuracy of proposed formulation appear to be the same as the previous HDG FSI formulation.

The new formulation is shown to approach a 50% reduction in global DOF count for high-order simulations for an arbitrary FSI problem. For the specific numerical example of the Turek and Hron benchmark using only Q2 elements, the new formulation is shown to match the results of the original formulation with a negligible change in accuracy, while the number of total global DOFs is reduced by 17% and the number of total local DOFs is reduced by 25%. This work will form the basis for future studies, namely an empirical efficiency study to determine the efficiency of this method when applied to large problems.

Acknowledgments

J. Sheldon gratefully acknowledges financial support from Naval Sea Systems Command, Advanced Submarine Systems Development Office, Mr. Patrick Tyler (SEA073). S. Miller and J. Pitt acknowledge internal support for this research from the Applied Research Laboratory at The Pennsylvania State University.

Appendix A: Fluid domain DOF reduction

This appendix demonstrates the fluid domain DOF reduction of the HDG FSI formulation presented in this work over the HDG FSI formulation previously presented in [3, 4]. These formulations are respectively referred to as "new" and "old" for brevity in the remainder of this appendix. Lagrange polynomials are used as basis functions in this example, but the concept extends to other basis functions with similar results. In the following equations and table, the variables $d =$ dimension, $k =$ polynomial order, $f =$ unique faces in the fluid domain[¶], and $c =$ cells in the fluid domain.

The number of fluid domain DOFs for an arbitrary HDG FSI are presented below for both the old and new formulations, along with the DOF reduction of the new formulation over the old.

[¶]The fluid domain includes both the fluid and mesh DOFs, even though only the mesh DOFs are reduced by the new formulation.

Local DOFs with old formulation: $N_{lo}=c(2d^2+2d+1)(k+1)^d$.

Local DOFs with new formulation: $N_{ln}=c((k+1)^d+(d^2+d)((k+1)^d+2^d))$.

Global DOFs with old formulation: $N_{go}=2fd(k+1)^{d-1}+c$.

Global DOFs with new formulation: $N_{gn}=fd((k+1)^{d-1}+2^{d-1})+c$.

Local DOF reduction from old to new: $$R_l=1-\frac{N_{ln}}{N_{lo}}=\frac{\left(d^2+d\right)\left(1-2^d(k+1)^{-d}\right)}{2d^2+2d+1}.$$

Global DOF reduction from old to new: $$R_g=1-\frac{N_{gn}}{N_{go}}=\frac{1}{2}-\frac{(k+1)\left(c+2^d df\right)}{2\left(ck+c+2df(k+1)^d\right)}.$$

Applying this to specific values of d and k yields the results in Table 4, which show that as polynomial order increases, the local and global percent DOF reduction of the new formulation over the old approaches approximately 50%.

Table 4: The fluid domain DOF reduction from the new HDG FSI formulation over the old formulation; $f=cd$ for the finite R_g values. The limit as $k\to\infty$ is exact.

	$k=2$	$k=3$	$k=4$	$k=5$	$\lim_{k\to\infty}$
R_l for $d=2$	25.64%	34.62%	38.77%	41.03%	46.15%
R_l for $d=3$	33.78%	42.00%	44.93%	46.22%	48.00%
R_g for $d=2$	16.00%	24.24%	29.27%	32.65%	50.00%
R_g for $d=3$	27.61%	37.37%	41.91%	44.38%	50.00%

References

[1] M. Heil, An efficient solver for the fully coupled solution of large-displacement fluid–structure interaction problems, Computer Methods in Applied Mechanics and Engineering, 193 (2004), 1–23.

[2] T. Dunne, R. Rannacher, T. Richter, Numerical simulation of fluid-structure interaction based on monolithic variational formulations, Fundamental Trends in Fluid-Structure Interaction, 1 (2009), 1–75.

[3] J. P. Sheldon, A hybridizable discontinuous Galerkin method for modeling fluid-structure interaction, Ph.D. thesis, The Pennsylvania State University, (2016).

[4] J. P. Sheldon, S. T. Miller, J. S. Pitt, A hybridizable discontinuous Galerkin method for modeling fluid–structure interaction, submitted for publication consideration on Feburary 15th, 2016.

[5] B. Cockburn, G. E. Karniadakis, C.-W. Shu, The development of discontinuous Galerkin methods, Springer, 2000.

[6] B. Cockburn, J. Gopalakrishnan, R. Lazarov, Unified hybridization of discontinuous Galerkin, mixed, and continuous Galerkin methods for second order elliptic problems, SIAM Journal on Numerical Analysis, 47 (2) (2009), 1319–1365.
[7] J. P. Sheldon, S. T. Miller, J. S. Pitt, Methodology for comparing coupling algorithms for fluid-structure interaction problems, World Journal of Mechanics, 4 (2014), 54–69.
[8] N. Nguyen, J. Peraire, B. Cockburn, A hybridizable discontinuous Galerkin method for Stokes flow, Computer Methods in Applied Mechanics and Engineering, 199 (9) (2010), 582–597.
[9] N. C. Nguyen, J. Peraire, Hybridizable discontinuous Galerkin methods for partial differential equations in continuum mechanics, Journal of Computational Physics, 231 (18) (2012), 5955–5988.
[10] J. Payne, M. Barone, S. N. Laboratories, U. S. D. of Energy, U. S. D. of Energy. Office of Scientific, T. Information, Methods for Simulation-based Analysis of Fluid-structure Interaction, United States. Department of Energy, 2005.
URL https://books.google.com/books?id=jS-RAQAACAAJ
[11] G. Hou, J. Wang, A. Layton, Numerical methods for fluid-structure interaction — a review, Communications in Computational Physics, 12 (2) (2012), 337–377. doi:10.4208/cicp.291210.290411s.
[12] Y. Bazilevs, K. Takizawa, T. E. Tezduyar, Front Matter, John Wiley & Sons, Ltd, 2013, pp. i–xix. doi:10.1002/9781118483565.fmatter.
URL http://dx.doi.org/10.1002/9781118483565.fmatter
[13] L. Heltai, S. Roy, F. Costanzo, A fully coupled immersed finite element method for fluid structure interaction via the deal. ii library, Archive of Numerical Software, 2 (1) (2014), 1–27.
[14] S. Roy, L. Heltai, F. Costanzo, Benchmarking the immersed finite element method for fluid–structure interaction problems, Computers & Mathematics with Applications, 69 (10) (2015), 1167–1188.
[15] T. Richter, T. Wick, Finite elements for fluid–structure interaction in ALE and fully Eulerian coordinates, Computer Methods in Applied Mechanics and Engineering, 199 (41) (2010), 2633–2642.
[16] T. Wick, Solving Monolithic Fluid-Structure Interaction Problems in Arbitrary Lagrangian Eulerian Coordinates with the deal. II Library, Universitätsbibliothek der Universität Heidelberg, 2011.
[17] M. Gurtin, E. Fried, L. Anand, The mechanics and thermodynamics of continua, Cambridge University Press, 2009.
[18] A. Spencer, Continuum mechanics, Dover Publications, 2004.
[19] E. Süli, D. F. Mayers, An introduction to numerical analysis, Cambridge university press, 2003.
[20] N. C. Nguyen, J. Peraire, B. Cockburn, An implicit high-order hybridizable discontinuous Galerkin method for the incompressible Navier–Stokes equations, Journal of Computational Physics, 230 (4) (2011), 1147–1170.
[21] S.-C. Soon, B. Cockburn, H. K. Stolarski, A hybridizable discontinuous Galerkin method for linear elasticity, International Journal for Numerical Methods in Engineering, 80 (8) (2009), 1058–1092.
[22] M. Kronbichler, W. A. Wall, Hybridized discontinuous Galerkin discretizations for flow problems.
URL https://mediatum.ub.tum.de/doc/1171537/1171537.pdf

[23] S. Turek, J. Hron, Proposal for numerical benchmarking of fluid-structure interaction between an elastic object and laminar incompressible flow, Fluid-Structure Interaction, (2006), 371–385.
[24] V. S. Ryaben'kii, S. V. Tsynkov, A theoretical introduction to numerical analysis, CRC Press, 2006.
[25] W. Bangerth, T. Heister, G. Kanschat, `deal.II` Differential Equations Analysis Library, Technical Reference.
URL `http://www.dealii.org`
[26] W. Bangerth, T. Heister, L. Heltai, G. Kanschat, M. Kronbichler, M. Maier, B. Turcksin, T. Young, The `deal.ii` library, version 8.2, Archive of Numerical Software, 3 (100).